Summary of Doctoral Dissertation
Doctoral Program in Managment, Production and Design (37^{th}cycle)

Laser finishing of components by Directed Energy Deposition

Experimental campaigns and numerical simulations

By

Giuseppe Vecchi

******

Supervisor(s):
Prof. Eleonora Atzeni, Supervisor
Prof. Alessandro Salmi, Co-Supervisor

Politecnico di Torino
September 2025

Contents

Chapter 1

Directed Energy Deposition: strengths and weaknesses

Additive manufacturing (AM) knew a rapid growth across manufacturing industry over the last decades, from being used only for prototyping purposes to providing market-ready components. Different manufacturing processes fall under the definition of AM. One of the most noteworthy process, both currently and in the near future, is Directed Energy Deposition (DED), primarily due to its high flexibility, large building volumes and fast deposition rates. However, a wider use of Directed Energy Deposition is still hindered by unsolved problems, such as low geometrical accuracy and poor surface quality.

1.1 Directed Energy Deposition Background Information

DED is one of the seven processes AM is conventionally divided into [1], and one of the most promising limiting to metallic materials. DED systems use a focused energy source to locally melt a substrate. Feedstock materials are delivered inside the melt pool, melting in turn. The energy source and the feedstock delivery system compose the deposition head, core element of any DED machine. The present document is limited to DED systems employing a laser beam as the energy source and metallic powder as the feedstock material (DED-LB/Powder), as they account for the vast

Fig. 1.1 Worn automotive die before and after the repair by DED-LB/Powder [7].

majority of installed systems [2, 3]. The relative motion between deposition head and substrate enables the almost instantaneous solidification of previously melted material, laying the foundations to the growth of the component [4].

DED has been considered for repairing activities in several published studies as a possible alternative to arc welding techniques. It has been confirmed that the repairing through DED-LB/Powder implies a lower environmental footprint than producing a component from scratches, especially when dealing with bulk components such as mould's shell [5, 6]. Furthermore, Bennet *et al.* [7] compared the results of the remanufacturing of a worn automotive die by DED-LB/Powder and TIG welding, results of showed in Figure 1.1. They reported that the die repaired by DED-LB/Powder showcased a useful life similar to the original one, whereas the TIG repaired one only lasted for around 20% of the original length, helping to reduce the estimated environmental footprint.

In conclusion, DED-LB/Powder meets all the requirements to be profitably used in the repair and remanufacturing field. That being said, a broader industrial usage of DED-LB/Powder is still hindered by several process restrictions. DED-LB/Powder systems usually show modest geometrical accuracy, induce considerable residual stresses in deposited components, and do not ensure a satisfying surface quality. The poor surface quality of DED-LB/Powder components is well known, usually leading to Ra values between 25 and 35 µm [8]. The adverse role of high surface roughness on tribological, corrosion resistance and fatigue properties of a component are now largely established [9]. Thus, it is straightforward to understand how post-deposition surface finishing processes are mandatory to ensure the desired mechanical properties to DEDed components.

1.2 Surface Finishing of Components by Directed Energy Deposition

1.2.1 Mechanical Finishing Processes

Mechanical finishing processes are a set of surface finishing techniques that use mechanical energy to transform the surface layer of a component. These processes can either remove the outermost layer of a component, or induce a local plastic deformation. Limiting to material removal processes, mechanical surface finishing processes can be further classified according to the tool used to remove the outermost material layer. The simplest classification that can be made is between processes that employ tools with defined geometries, such as milling or turning, and those using tools without defined geometries, such as grinding, mass finishing and abrasive finishing. Milling and turning are able to finishing components in limited time periods, concurrently achieving excellent surface quality. Moreover, multi-axis CNC machining enables the processing of complex geometries, not being limited to axial-symmetric shapes. However, multi-axis CNC machining can have difficulties in handling the most intricate geometries resulting from AM processes. Mass finishing, abrasive finishing and grinding are usually used to either reach superior surface finishing, and therefore applied after a previous CNC machining phase, or when the complexity of the geometry to handle is outside the capabilities of multi-axis CNC machining.

1.2.2 Chemical Finishing Processes

Chemical finishing processes use chemical reactions to modify the surface of the material in exam. Chemical finishing treatments are well suited for AM components since they can easily reach any point of the surface, with no limitations caused by internal features or thin walls [10, 11]. Moreover, no contact tools are involved and no residual stresses induced in the part [12].

1.2.3 Thermal Finishing Processes

Laser finishing processes remelts the outermost deposited layer of the material in exam, smoothing its surface through surface tension and gravity, without affecting its bulk properties [13], as depicted in Figure 1.2. Laser polishing exhibits high degree of flexibility, being able to selectively melt part of a surface leaving the remaining untouched [14]. Moreover, it does not involve a physical tool, by-passing all the issues related to material hardness and tool wear. No lubricants or cooling fluids are required during LP operations, clearly distinguishing it from CNC machining. The absence of auxiliary fluids can be helpful in reducing the environmental impact of the process, and enables an easier integration between manufacturing and finishing operations.

In a DED-LB system there is already a laser suitable for LP operations, without the need of additional equipment. Therefore, the combination of DED-LB and LP might take place in the same system, using the same laser for both manufacturing steps, and strongly shortening the supply chain of the specific component. Since no lubricants are required by the LP treatment, not preventing further depositions on the substrate, LP and DED can be effectively alternated. Several works already investigated the suitability of LP to reduce the extreme roughness, and waviness, of DEDed components using the same laser for both manufacturing phases.

Rosa *et al.* [15] LPed AISI 316L samples deposited by DED-LB/Powder. They achieved a drastic 95% reduction of samples Sa, lowering it from 21 to 0.8 µm. Dos Santos Paes *et al.* [16] LPed samples deposited out of IRON AHC 100.29 and IN625, and compared the resulting surface improvements using both Ra and Wa. Iron samples showed a 30% Ra reduction, whereas inconel ones a more consistent 70% Ra reduction. Hodgir *et al.* [17] deposited and LPed samples of CPM-9V

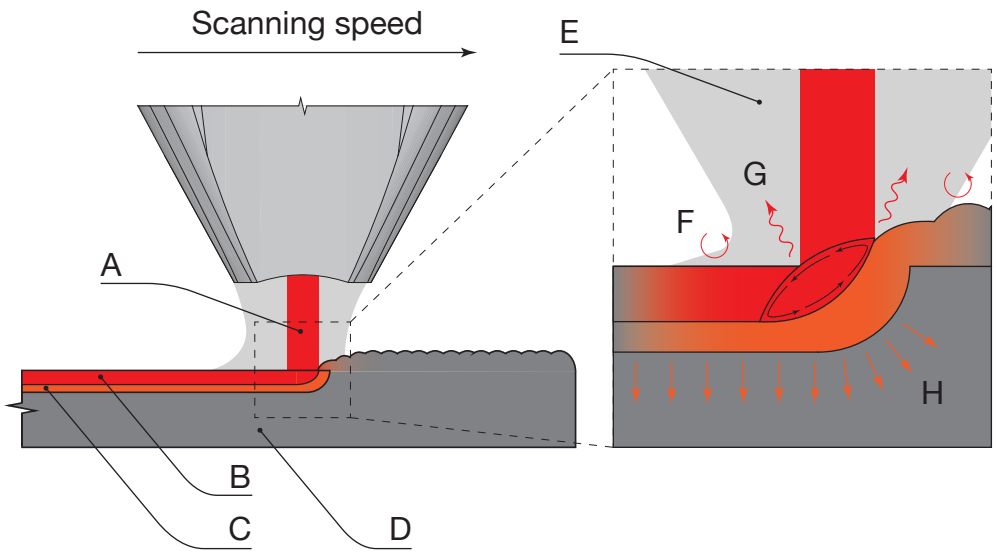

Fig. 1.2 Continuous-wave Laser Polishing scheme: A) continuous wave laser; B) remelted layer; C) heat affected layer; D) unaffected material; E) shielding gas; F) convection heat flow; G) radiation heat flow; H) conduction.

crucible steel, remarkably decreasing Ra from around 80 to 20 µm, standing a 73% Ra resduction. Cho *et al.* [18] investigated the influence of laser power, tracks overlap, and scanning strategy on the surface quality of 316L samples deposited by DED-LB/Powder. Ra decreased from 15.64 to 1.5 µm, mainly influenced by laser power and overlap. Bruzzo *et al.* [19] used a central-composite design (CCD) to investigate the influence of laser power, tracks overlap and laser incident angle on the resulting $S_{a,sf}$ and $S_{a,lf}$, areal counterparts of Ra and Wa respectively. They managed to reduced $S_{a,sf}$ from 10.35 down to 1.82 µm and $S_{a,lf}$ from 9.57 down to 3.97 µm.

In conclusion, several surface finishing processes might be used to improve the poor quality of DEDed components. Overall, LP processes here described seem to offer good surface quality without material waste and without the need of additional instrumentation outside the DED-LB system already at use [20]. However, an holistic experimental campaign is still lacking on the topic. Although the presented studies perfectly showed the capabilities of LP treatments, no clear factor screening campaigns have been performed, and no empirical models proposed to quantitatively correlate profile parameters to the process parameters investigated. Moreover, most of the studies in the field only referred to Ra and Sa, overlooking the potential information that other profile parameters might have embodied.

Chapter 2

Roughness Minimisation Campaign

Experimental campaigns have always been the first step for the understanding of an industrial process from an engineering standpoint. Observing a phenomenon, and trying to correlate its behaviour to its direct causes, sometimes can be more difficult than expected. In Section 2.1 the equipment used throughout the experimental campaign is presented. Section 2.2 describes the first exploratory campaign, whose main objective was the distinction of the active process parameters from the inactive ones. Finally, section 2.3 covers the optimisation campaign that followed the exploratory campaign. During the optimisation campaign the focus moves to the definition of an set of parameters granting the optimal response of the system under investigation, a minimum of Ra in this case.

2.1 Experimental Equipment

The DED-LB/Powder system used in this study was the Laserdyne® 430, 5-axis commercial DED system provided by Prima Additive (Torino, Italy). The Laserdyne® 430 system was equipped with the Advanced Head, featuring four radially distributed nozzles around the central laser beam. In the configuration used in this study, the focal plane of the powder stream and of the laser beam were disposed on the same plane at 8 mm from the nozzle. The laser module coupled with the system was the CF 1000 by Convergent Photonics (Torino, Italy), Yb fibre laser with a maximum power of 1 kW and nominal wavelength equal to (1075 ± 3) nm. The MetcoAdd 316L-D by Oerlikon (Freienbach, Switzerland) was the feedstock material used

for sample deposition. The MetcoAdd 316L is a gas atomised austenitic stainless steel with a granulometry in the range from 45 to 106 µm. The Leica S9i stereo-microscope, by Leica (Wetzlar, Germany) was employed for image acquisition and qualitative surface characterisation. The Leica S9i provides a 10 MP resolution on the focal plane, with a pixel size of (1.67×1.67) µm^2, and a high magnification of up to 55×. Moreover, Leica's FusionOptics technology also grants a 12 mm depth of focus, drastically facilitating the use of the instrument. The RTP-80, by SM Metrology Systems (Volpiano, Italy), was the roughness tester used for surface profile extractions and perform consecutive quantitative quality assessments. The RTP-80 is a stylus-based roughness tester that offers a 0.001 µm resolution over a ±500 µm measuring range.

2.2 Exploratory Campaign

The main objective of the exploratory campaign described in this section was the definition of which LP process parameters exert a significant influence on the quality of the surface following the completion of the treatment. Consequently, it is essential to define several aspects of the exploratory campaign in advance.

The initial step is to define the response variable of the system, which will be used to assess the quality of the outcomes achieved. Therefore, the exploratory campaign considered Ra, Rz, Rsk and Rku, along with their corresponding waviness parameters, aiming at an holistic description of surface topographies. However, despite measuring and recording several parameters, Ra was chosen as the primary response variable, guiding the decisions made during the experimentation. The prominent role of Ra in scientific literature, international standards and real-life industrial applications made it impossible to opt for another profile parameter. Secondly, the parameters to investigate must be identified too. Table 2.1 reports the four process parameters considered for investigation. In particular, Linear Energy Density (LED) is defined as the ratio between laser power and travelling speed of the deposition head. h_d is the hatching distance, namely the distance between two consecutive laser polishing tracks. S_d is the stand-off distance of the deposition head with respect to the surface to finish. The S_d indirectly controls the diameter of the laser spot using during LP treatments. Finally, V_{Ar} is the argon flow rate used as shielding gas in the study. The experimental campaign was organised as a 2-level full-factorial campaign with

Table 2.1 Levels of the investigated factors.

Factor	Low level	High level	Central point
LED/(J mm^{-1})	21	70	45.5
h_d/(mm)	1	2	1.5
S_d/(mm)	8	28	18
V_{Ar}/(L min^{-1})	2	10	6

three replications of each factorial point. 2-level campaign are largely used in factors screening campaign and exploratory campaigns due to their extreme material efficiency. A full-factorial design was opted over a fractional one to have a clear visualisation of all possible interactions between investigated process parameters. Five replications of the central point of the design were also added for a first estimate of non-linear effects. Overall, 53 experimental runs were performed during the exploratory campaign. The LP treatments were performed in a randomised order

The Leica S9i was used to capture pictures of the each treatment, and the RTP-80 used for roughness evaluation. Five roughness measurements were taken, both along the direction of polishing tracks (x direction) and perpendicularly to it (y direction), as shown in Figure 2.1. Upon close inspection, it appears that $Ra_{\perp}$ consistently exhibits higher values than its parallel counterpart, suggesting that the perpendicular direction was the most critical of the two. In fact, ISO 21920-3 [21] emphasises the importance of considering the direction of higher roughness when performing surface characterisation procedures. Additionally, a correlation analysis was performed to enhance a finer understanding of the relationship between $Ra_{\perp}$ and $Ra_{\parallel}$. The correlation analysis resulted in a Spearman correlation coefficient of $r_s = 0.752$, computed at a 95% confidence level, suggests a strong correlation between the rankings. This result was considered of the utmost importance since it ensures that LP treatments could be similarly ranked using both $Ra_{\perp}$ and $Ra_{\parallel}$. Therefore, the present study focused only on the perpendicular parameters acquired, being confident that no meaningful differences were overlooked.

The same results were also analysed by means of an ANOVA, whose main effect plots are schematically represented in Figure 2.2. It is straightforward to notice how a high energy density resulted in better surface quality after LP treatments. In particular, high levels of LED and low levels of h_d and S_d ensure lower $Ra_{\perp}$ at end

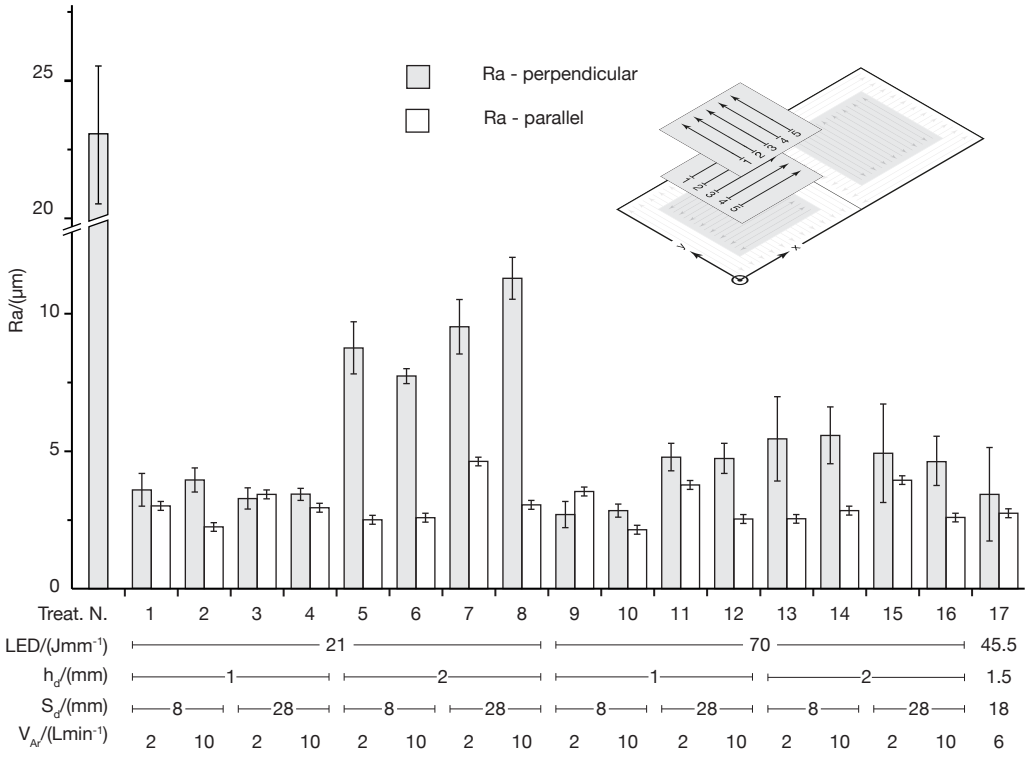

Fig. 2.1 Exploratory campaign results for Ra.

of the treatment. On the other hand, V_{Ar} changes do not have a meaningful influence on $Ra_{\perp}$.

Finally, Equation 2.1 describes the linear model that was drawn from the ANOVA. The linear model provided a leaner equation than complete model, at a cost of a slightly lower accuracy, $R^2 = 64.85\%$.

$$Ra_{\perp} = 1.259 - 0.0404 \cdot LED + 3.550 \cdot h_d + 0.0374 \cdot S_d + 0.0184 \cdot V_{Ar} \qquad (2.1)$$

2.3 Optimisation Campaign

The culminating moment of any experimental activity is the definition of an optimal working condition, granting the best answer from the system studied. Optimization campaigns fulfil this role, with the aim of providing an accurate empirical model that mathematically describes the behaviour of the system in the region of interest.

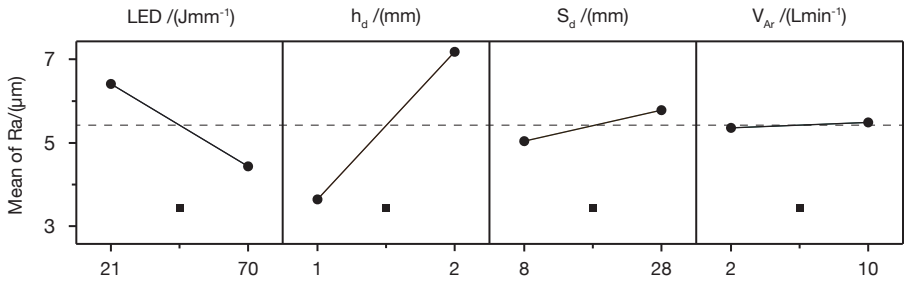

Fig. 2.2 Main effect plots for $Ra_{\perp}$

During the exploratory campaign LED, h_d and S_d were identified as the active factors, being able to influence the quality of the LPed surfaces. More in detail, high LED and low h_d led to low Ra values, showing room for further surface quality improvement. S_d was an active factor, but detrimental for the quality of the final surface. Conversely, V_{Ar} did not had almost any influence on the response variable, therefore being considered not active. Therefore, only LED and h_d were considered in this phase, as S_d and V_{Ar} were not deemed eligible for further optimisations. Therefore, the first step of the optimisation campaign was the process improvement one. In a process improvement phase the active factors are varied to identify a domain hosting a possible optimum of the response function. As only two parameters were considered at this stage, the process took place in a bi-dimensional domain, strongly simplifying the mathematical structure of the investigation.

The steepest descent was the algorithm chosen for the process improvement phase. Figure 2.3 presents the level curves for the linear model presented in Equation 2.1. The direction of the steepest descent path is graphically represented by the perpendicular to the level curves, as depicted in Figure 2.3 too. Finally, the angular uncertainty was computed and it is shown in Figure 2.3 as a grey cone.

The results of the steepest descent algorithm are represented in Figure 2.4. Three replications of each steepest descent step were carried out, and the results were aggregated in terms of means and standard deviations. $Ra_{\perp}$ results were used to take actions and halt the steepest descent algorithm when a possible optimal region was identified. In addition, other R and W-parameters were measured and reported to provide a holistic description of the transformations that the samples underwent. $Ra_{\perp}$ exhibited a monotonic trend, with a gradual decrease over the four steps. However, the amount of the $Ra_{\perp}$ improvement decreased at each step, dropping below 10% at the fourth step. At that point, the $Ra_{\perp}$ improvement was comparable with the

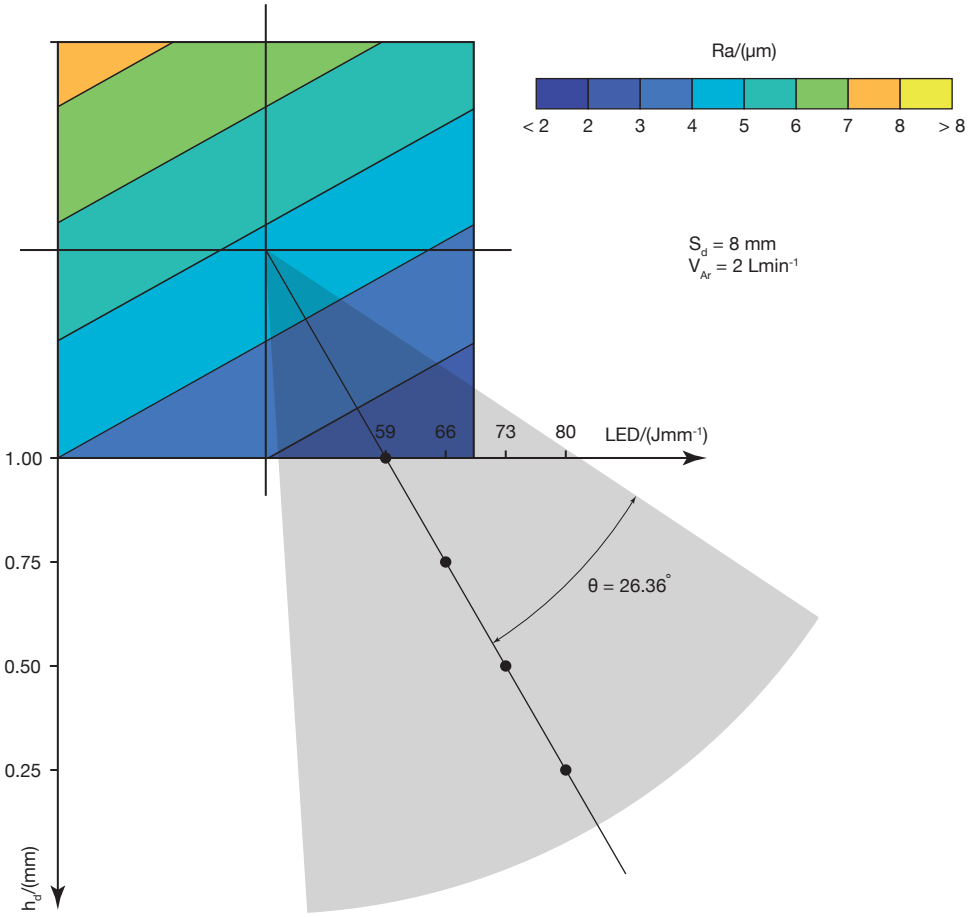

Fig. 2.3 Steepest descent path for considering LED and h_d. V_{Ar} equal to $2\,\mathrm{L/min}$ and S_d equal to $8\,\mathrm{mm}$.

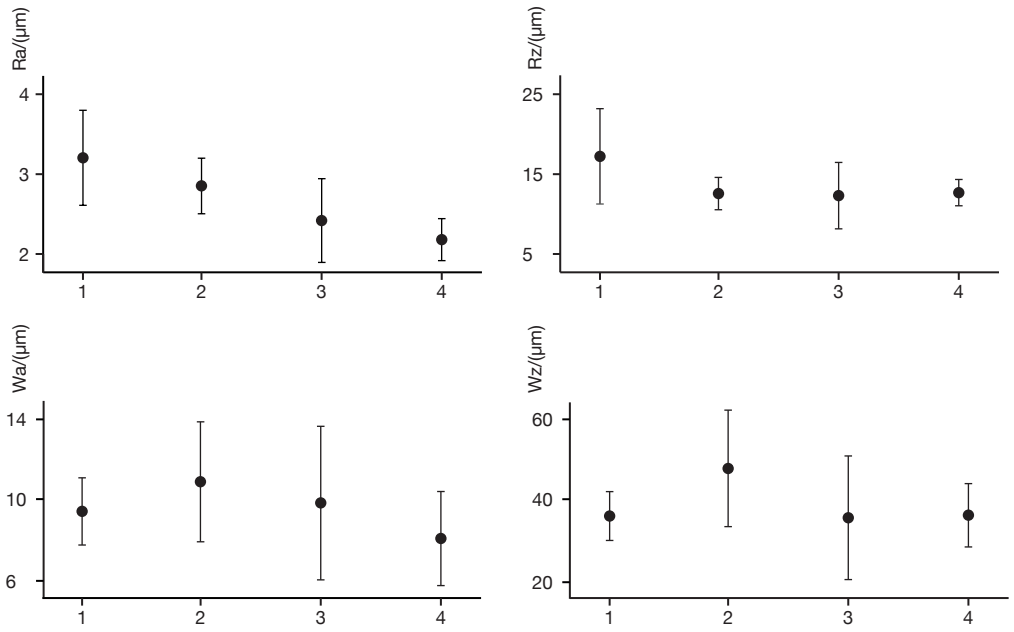

Fig. 2.4 Results of the steepest descent algorithms in terms of $Ra_\perp$, $Rz_\perp$, $Wa_\perp$ and $Wz_\perp$.

measured standard deviation, suggesting that a possible region of optimum was reached. The data provided by $Wa_\perp$ and $Wz_\perp$ were not deemed to be of sufficient utility. $Wa_\perp$ remained within the same range of (8.5 ± 2)µm, comparable to the the best values measured during the exploratory campaign. Similarly, also $Wz_\perp$ resulted in values comparable to the exploratory campaign. On the one hand this results can hinder the hope for further improving surface waviness of LPed samples. On the other hand, it appears that higher energies did not result in increased waviness of the sample, counterbalancing eventual roughness improvements that might have been observed.

In conclusion, the impossibility to indefinitely decrease h_d, together with always smaller $Ra_\perp$ improvements, suggested the possibility of halting the steepest descent method at its fourth step. Therefore, the pair of LED = 80 J mm^{-1} and h_d = 0.25 mm was selected as the central value for a further optimisation campaign, aiming at computing a model to accurately describe the linear and non-linear effects of LED and h_d.

Table 2.2 Levels of the investigated factors

	Low level -1	Intermediate level 0	High level 1
LED/(J mm^{-1})	76	81	86
h_d/(mm)	0.10	0.25	0.40
S_d/(mm)		8	
V_{Ar}/(L/min)		2	

2.3.1 ANOVA for Ra

A 3-level full factorial design was chosen for the optimisation campaign. 3 levels allows the accurate detection of non-linear effects, at a cost of a higher number of factorial points to test. Three replicates of each factorial point were performed for higher reliability, resulting in a total of 27 experimental runs. Table 2.2 shows the levels of LED and h_d used during the optimisation campaign.

The ANOVA for Ra conducted on the results of the optimisation campaign provided the model reported in Equation 2.2. The model highlight the high influence on non linear terms on the value of the response variable, namely the contribution of h_d^2.

$$Ra = 0.57 + 0.0324 \cdot LED + 2.87 \cdot h_d + 12.88 \cdot h_d^2 - 0.1284 \cdot LED \cdot h_d \qquad (2.2)$$

Figure 2.5 depicts the response surface of Ra. On the left-hand side of the picture the three dimensional plot is reported, whereas on the right-hand side there is the representation of the corresponding level curves. The level curves are extremely helpful in highlighting the areas of optimal response of the system.

2.3.2 ANOVA for Wa

Passing to Wa, the model proposed by the ANOVA is reported in Equation 2.3. Differently form Equation 2.2, this second model considers both quadratic terms, LED^2 and h_d^2, but does not consider the interaction between main effects. However, the model proposed by Equation 2.3 has extremely limited R^2_{pred}, lower than 10%.

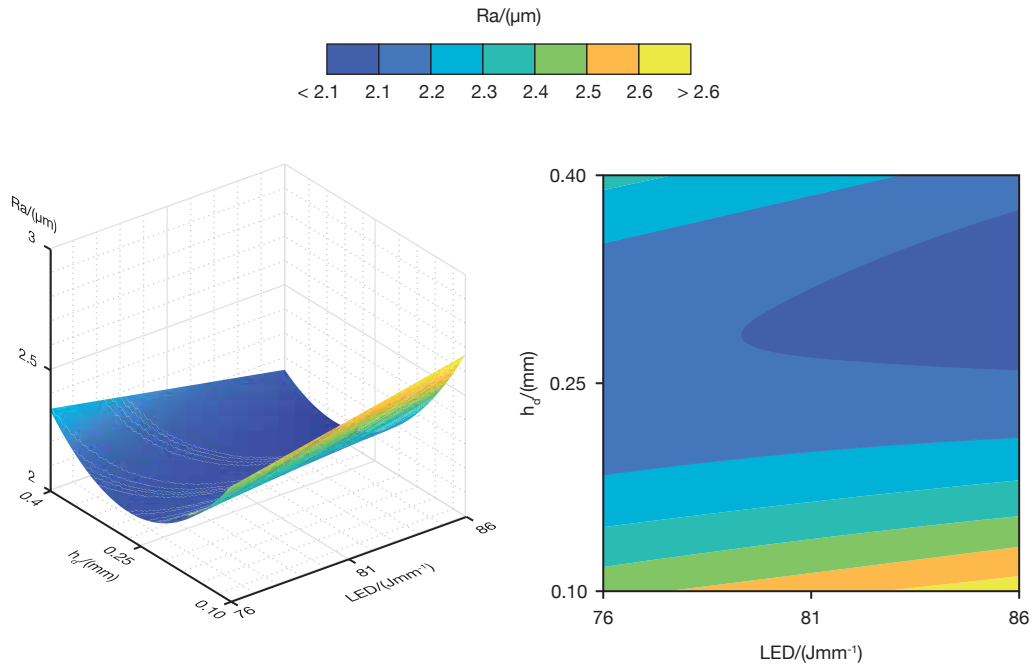

Fig. 2.5 Surface and contour plots for Ra.

This strongly established the inadequacy of the Wa model to predict new values in the region of interest, drastically hindering its applicability. The surface plot of Wa was depicted in Figure 2.6 nonetheless. The prominent role of second-order effects is clearly depicted buy the shape of the surface, characterised by the presence of saddle point at the centre of the region of interest. Although the information provided by the graph should be carefully handled, due to the low prediction capabilities of the model, it may still be useful for the present investigation. The region defined by intermediate h_d values and high LED values is one of the two regions leading to the lowest Wa, always limited to the region of interest. This same region was already identified as an optimal response region for Ra.

$$Wa = -190 + 5.03 \cdot LED - 30.2 \cdot h_d - 0.0314 \cdot LED^2 + 66.3 \cdot h_d^2 \qquad (2.3)$$

Figure 2.7 displays the Wa curve level overlayed on the Ra curve levels, and highlights a region where both response variables are minimised simultaneously. By computing the gradient of the 2-order model resulting from the Ra ANOVA, it was possible to define the optimal set of parameters, namely LED = 86 J mm^{-1} and h_d =

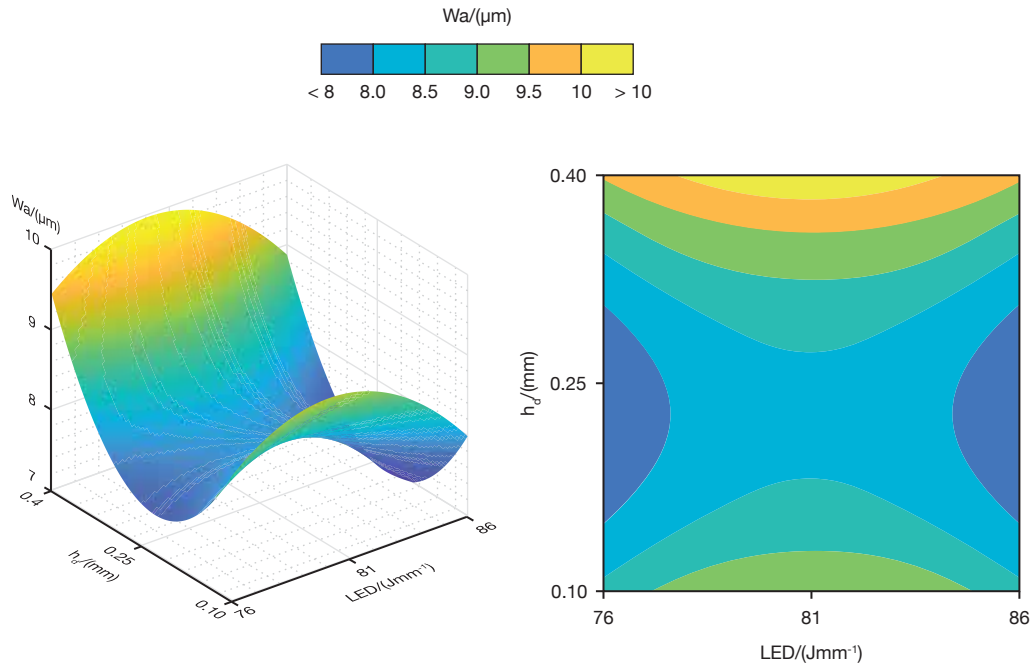

Fig. 2.6 Surface and contour plots for Wa.

0.32 mm, leading to a $Ra_{\perp}$ mean value of 2.06 µm. The confidence interval (CI) of the same mean value was found to be $(1.93, 2.18)$ at a confidence level of 95%.

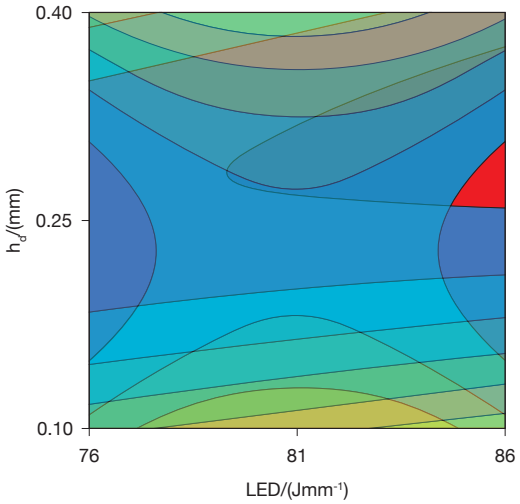

Fig. 2.7 Overlay of *Wa* and *Ra* curve levels.

Chapter 3

Induced Residual Stresses

Every manufacturing process, either casting, forging or machining, induces a residual stress state in the component at the end of the same process. Residual stresses play a major role in AMed components, especially due to the high thermal gradients and cooling times typical of AM processes [22]. Although residual stress are difficult to detect by definition, they must be considered when evaluating the performances of a component [23]. Large residual stresses can induce consistent distortions in the component, preventing it from reaching the required geometrical accuracy [22]. In addition, residual stresses can be highly detrimental in terms of stress corrosion and fatigue life, both of single components and of welded joints [23, 24]. For these reasons, residual stress measurement was the first activity carried out to define the collateral effects of LP on the substrates.

3.1 Experimental Equipment

Numerous methods are today available to measure residual stress states across the section of a component, not being limited to surface values. The strain gauge method is surely the most widespread across industry, due to its simplicity and reliability [25, 23].

The procedure is based on the drilling of a hole at the surface location that is to characterise. The drilling removes part of the material of the component, and therefore breaks the internal residual stress equilibrium. The redistribution of the residual stresses around the hole brings to a deformation of the same material. If the

residual stresses were tensile stresses, the diameter of the hole would be enlarged compared to the nominal one. On the other hand, compressive residual stresses would result in a hole smaller than the nominal one. The deformations of the hole induced by the residual stress state are usually very small, and require appropriate instrumentation to be detected and registered during the hole drilling. A strain gauge rosette is usually used to measure the deformation of the material in the surrounding of the hole.

In the present investigation the strain gauge rosette used was the 1-RY61-1.5/120R3 by HBM (Darmstadt, Germany). Each rosette was glued on the the LPed surface of the sample. The pneumatic system used to drill the hole into the strain gauge was the MTS3000 - Restan by SINT technology (Calenzano, Italy). The MTS3000 uses a air turbine put in rotation the mini-end mill used for the drilling operation. More in detail, the end mill was a 1-SINTCTT2/1, carbide inverted cone endmill by SINT technology. The signals from the rosette were acquired and amplified by the QuantumX MX440 by HBM. Data amplified by the QuantumX were gathered in a desktop PC using the RSM 7.13 software package by SINT technologies, and later processed using the EVAL 8 software environment by the same SINT technologies. EVAL software follows the procedure outlined in the ASTM E837, which provides a meticulous description of the entire procedure. Data elaboration resulted in the computation of σ_{min}, σ_{max} and β as a function of z, namely the depth under sample surface.

3.2 Experimental Campaign

The objective of this experimental campaign was to understand the influence of LP treatments on the residual stress of DEDed samples. Therefore, four additional samples were deposited. One sample was kept as reference, whereas the others were LPed using three sets of LED and h_d close to the optimal set defined in Chapter 2 (Table 3.1).

Figure 3.1 depicts the residual stresses measured on the as-built sample. The as-built sample showed consistent compressive stresses close to the surface of the sample, with a minimum value close to 150 MPa at the surface of the samples. Residual stress rapidly increased for increasing depths, becoming tensile stresses already at 0.03 mm from the LPed surface. The now tensile residual stresses kept

Table 3.1 LP process parameters used to finish the DEDed samples

	Sample No1	Sample No2	Sample No3
LED/(J mm^{-1})	76	81	86
h_d/(mm)		0.32	
S_d/(mm)		8	
V_{Ar}/(L/min)		2	

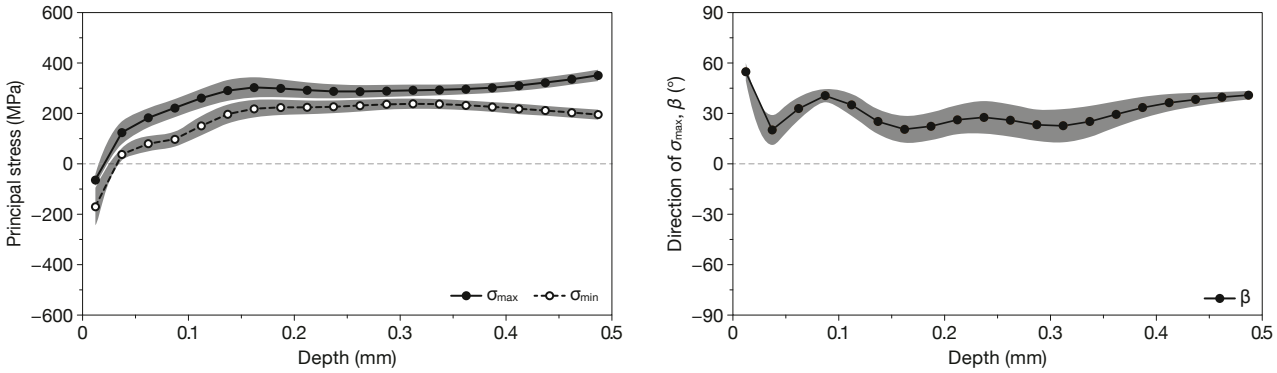

Fig. 3.1 Residual stresses measured on the sample maintained in as-built condition.

increasing until a depth of 0.15 mm, where a plateau was reached. From there on, the maximum tensile stress was found between 300 and 350 MPa.

The residual stress measurements carried out on the LPed samples are depicted in Figure 3.2. No significant differences were detected as far as the maximum stresses are considered. All three samples resulted in being featured by significant tensile stresses that slightly increased moving away from the LPed surface, as for the as-built samples. The Sample No2, LPed with a LED of 81 J mm^{-1}, was the only one to exhibit a different behaviour compared to the other samples. In particular, the minimum stress curve measured for the Sample No2 is very close to the maximum one. Conversely, Sample No1 and Sample No2 were featured by minimum stresses considerably lower than the respective maximum ones. Additionally, Sample No2 also exhibit slightly different β values, especially far from the surface. Further investigation would be required to understand if these differences could be explained by the LP or by some different initial condition of the sample after deposition.

However, some common conclusions can be drawn for all three LP conditions. The LP treatments seems to affect considerably the residual stress state of the LPed samples. In particular, the sample in as-built state showed compressive stress in

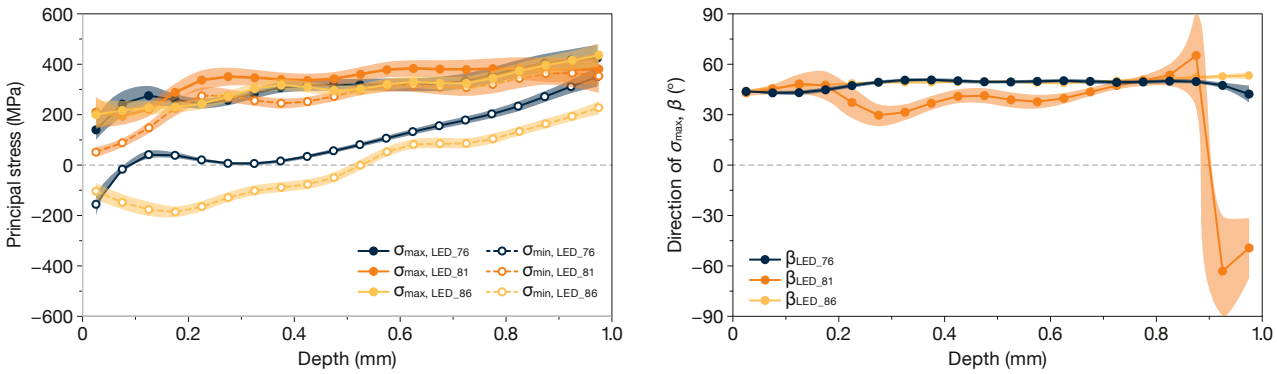

Fig. 3.2 Residual stresses measured on the LPed samples.

the sub-superficial region, whereas LPed samples all exhibited tensile stress in the same region. However, these differences seems only to affect the first 0.2 mm below the surface of the sample, with no meaningful influence on the core of the sample itself. This element suggests that appropriate stress relief heat treatments could profitable reduce, or eliminate at all, the residual stresses induced by LP as they already profitably do with DEDed samples [26].

Chapter 4

Numerical Modelling

The experimental activity described in the preceding chapters has proven useful for elucidating the physics of the LP under investigation. The results obtained from experimental trials strongly suggest a useful role of the LP in the post processing of DEDed components. However, all experimental campaigns share common limitations. The design and execution of an experimental campaign is a time consuming process, with a significant cost in terms of raw materials and other resources. Additionally, the results obtained are typically limited to the boundary conditions tested and may lack generality. Therefore, experimental activities can be paired with numerical simulation campaigns to provide a broader overview of the possible outcomes of the experimentation, substituting the real experimental trial when needed. In particular, the thermal model developed in this study provided a map of the temperatures inside the sample during the LP treatment. This information will enhance the understanding of material behaviour during the LP treatment and will help prognosticating further information such as the depth of the molten layer and of the heat affected zone.

4.1 Numerical Model

Abaqus CAE by Dassault Systemes (Vélizy-Villacoublay, France) was the software environment used to develop the numerical model proposed in this chapter. The model was a pure conductive model, not taking into account any possible motion of the molten metal due to convective forces. This hypothesis strongly simplifies

Table 4.1 LP process parameters used to finish the DEDed samples

Natural convective heat transfer/($W\,m^{-2}\,K^{-1}$)	20
Forces convective heat trasnfer/($W\,m^{-2}\,K^{-1}$)	100
Material emissivity/(-)	0.6
Absorbivity/(-)	0.32

the mathematical treatment of the problem, at a cost of a lower accuracy of the same model. The model simulated the same LP conditions that ensured the optimal response of the system during the experimental campaign, namely LED = $86\,J\,mm^{-1}$ and $h_d = 0.32\,mm$. Other significant coefficients are collected in Table 4.1.

The simulated platform was $100 \times 100 \times 8\,mm^3$. A $60 \times 30 \times 2\,mm^3$ was place at the centre of the upper surface of the platform, as it would in a real case scenario. The same $20 \times 20\,mm^2$ was considered for LP. Natural convection was applied on all free surfaces of the model. Forced convection was applied using the FILM subroutine following the motion of the deposition head during the LP treatment. Similarly, the laser was modelled as a surface heat flux impacting the sample on its upper surface. The motion of the heat source was modelled using the DFLUX subroutine, forcing it to follow the path of the deposition head during the LP treatment. The model used linear elements as the only objective of the simulation was the computation of the temperature field resulting from the LP treatment.

4.2 Experimental Validation

The results of the numerical model were compared with experimental results for validation. The same platform and sample geometries were used for a reliable comparison. Again, the optimal set of parameters was used for finishing the sample. Four thermocouples were welded on the platform for measuring the temperatures reached during the LP treatment. The location of the thermocouples is schematically presented in Figure 4.1. Thermocouple D was welded at the centre of the LP area, on the back of the platform.

Figure 4.2 depicts the temperatures reached at the four investigated points throughout the LP treatment. Although the numerical model was able to qualitatively predict the temperatures profiles at the four selected locations, some quantitative er-

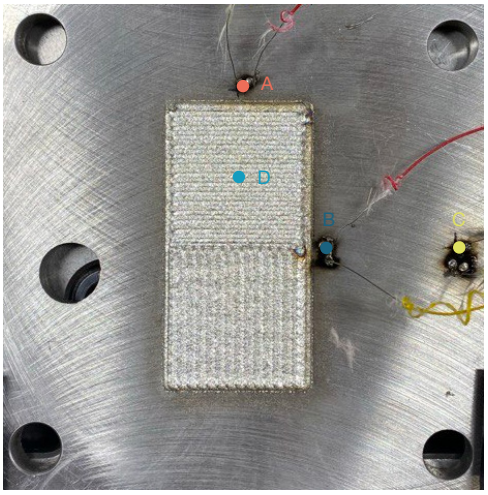

Fig. 4.1 Thermocouple placement on the platform. Sample presented before the LP process.

Table 4.2 Prediction error of the numerical model compared to the experimental data.

A	B	C	D
15.5%	33.5%	14.7%	-3.9%

rors are still present. Table 4.2 presents the error of the numerical model expressed as a percentage. A positive value indicates an overestimate of the temperature reached by the model, a negative value indicates an underestimate of the temperature reached by the model. It is clear that the prediction ability of the model greatly changes at different locations. The model well performed at location D, on the back of the substrate, whereas its accuracy decreases on the front of the platform, in particular at location B. This might be related to an incorrect modelling of the convective heat transfer between the platform and the environment, that will be objective of considerations in further studies.

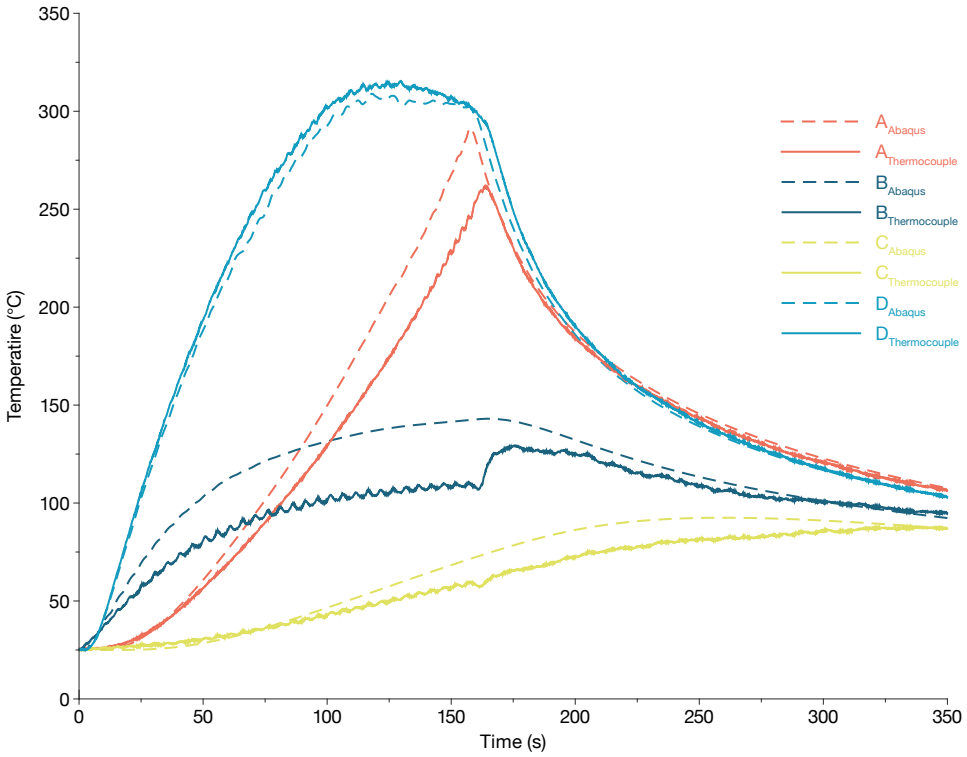

Fig. 4.2 Comparison of numerical and experimental data. Solid lines refers to experimental data, dashed lines refers to numerical data.

Chapter 5

Conclusions

The present work provides a comprehensive investigation into the potential of LP when coupled with DED-LB systems. While previous studies have demonstrated the feasibility of LP in DED components, no structured investigations have proposed a factor screening campaign followed by a properly designed optimisation campaign. Additionally, no considerations have been proposed to correlate the LP process to internal residual stress state modifications of the substrate.

Accordingly, the initial exploratory campaign was successful in identifying two active process parameters out of the four initially considered. Subsequently, the steepest descent algorithm was employed to search for a new optimal region, which was hypothesised to host a Ra minimum. Subsequently, an optimisation campaign identified the location of an optimum of both Ra and Wa, thereby minimising both the roughness and the waviness of the sample. In particular, the optimisation campaign resulted in a final Ra value of 2 µm, which is comparable to the Ra value achieved by rough machining finishing. This achievement justifies the interest in LP as it would allow the finishing of free surfaces without the need for additional machinery.

Additionally, residual stresses were evaluated for LP treatments in the vicinity of the identified minimum. The LP treatments resulted in alterations to the residual stress state of the samples at depths of up to 0.2 mm from the surface, with a transition from compressive to tensile residual stresses. Such alteration may prove problematic, as tensile residual stress in the vicinity of the sample surface could accelerate the failure of the component under periodic loading. However, as the DEDed sample

already requires a stress relief heat treatment, it can be assumed that no additional post-processing will be necessary for LPed samples.

A numerical model was finally proposed to estimate the temperature distribution inside a sample during an LP treatment. While comparison with experimental results was far from satisfactory, it did pave the way for further improvements in the future.

References

[1] ASTM international. Additive manufacturing – general principles – fundamentals and vocabulary. Standard ISO/ASTM 52900:2021, ISO, West Conshohocken, PA, 2021.

[2] Ian Gibson Ian Gibson. Additive manufacturing technologies 3d printing, rapid prototyping, and direct digital manufacturing, 2015.

[3] Gabriele Piscopo and Luca Iuliano. Current research and industrial application of laser powder directed energy deposition. *The International Journal of Advanced Manufacturing Technology*, 119(11-12):6893–6917, 2022.

[4] Gabriele Piscopo, Eleonora Atzeni, Abdollah Saboori, and Alessandro Salmi. An overview of the process mechanisms in the laser powder directed energy deposition. *Applied Sciences*, 13(1):117, 2022.

[5] J Michael Wilson, Cecil Piya, Yung C Shin, Fu Zhao, and Karthik Ramani. Remanufacturing of turbine blades by laser direct deposition with its energy and environmental impact analysis. *Journal of Cleaner Production*, 80:170–178, 2014.

[6] Joana R Gouveia, Sara M Pinto, Sara Campos, João R Matos, João Sobral, Sílvia Esteves, and Luís Oliveira. Life cycle assessment and cost analysis of additive manufacturing repair processes in the mold industry. *Sustainability*, 14(4):2105, 2022.

[7] Jennifer Bennett, Daniel Garcia, Marie Kendrick, Travis Hartman, Gregory Hyatt, Kornel Ehmann, Fengqi You, and Jian Cao. Repairing automotive dies with directed energy deposition: industrial application and life cycle analysis. *Journal of Manufacturing Science and Engineering*, 141(2):021019, 2019.

[8] Gabriele Piscopo, Alessandro Salmi, and Eleonora Atzeni. Investigation of dimensional and geometrical tolerances of laser powder directed energy deposition process. *Precision Engineering*, 85:217–225, 2024.

[9] Hamed Kalami and Jill Urbanic. Exploration of surface roughness measurement solutions for additive manufactured components built by multi-axis tool paths. *Additive Manufacturing*, 38:101822, 2021.

[10] Jun Ge, Selvum Pillay, and Haibin Ning. Post-process treatments for additive-manufactured metallic structures: a comprehensive review. *Journal of Materials Engineering and Performance*, 32(16):7073–7122, 2023.

[11] Haniyeh Fayazfar, Javid Sharifi, Mohsen K Keshavarz, and Mazyar Ansari. An overview of surface roughness enhancement of additively manufactured metal parts: a path towards removing the post-print bottleneck for complex geometries. *The International Journal of Advanced Manufacturing Technology*, 125(3):1061–1113, 2023.

[12] Jierui Mu, Tengteng Sun, Chu Lun Alex Leung, JP Oliveira, Yi Wu, Haowei Wang, and Hongze Wang. Application of electrochemical polishing in surface treatment of additively manufactured structures: A review. *Progress in Materials Science*, page 101109, 2023.

[13] Muhammad Arif Mahmood, Diana Chioibasu, Asif Ur Rehman, Sabin Mihai, and Andrei C Popescu. Post-processing techniques to enhance the quality of metallic parts produced by additive manufacturing. *Metals*, 12(1):77, 2022.

[14] Nikhil Nivrutti Kumbhar and AV Mulay. Post processing methods used to improve surface finish of products which are manufactured by additive manufacturing technologies: a review. *Journal of The Institution of Engineers (India): Series C*, 99:481–487, 2018.

[15] Benoit Rosa, Pascal Mognol, and Jean-Yves Hascoët. Laser polishing of additive laser manufacturing surfaces. *Journal of Laser Applications*, 27(S2), 2015.

[16] Luiz Eduardo dos Santos Paes, Milton Pereira, Fábio Antônio Xavier, Walter Lindolfo Weingaertner, Ana Sofia Clímaco Monteiro D'Oliveira, Erick Cardoso Costa, Louriel Oliveira Vilarinho, and Americo Scotti. Understanding the behavior of laser surface remelting after directed energy deposition additive manufacturing through comparing the use of iron and inconel powders. *Journal of Manufacturing Processes*, 70:494–507, 2021.

[17] Rajendra Hodgir, Ramesh K Singh, and Soham Mujumdar. Experimental investigation of laser remelting in directed energy deposition (ded) of cpm-9v. *Manufacturing Letters*, 35:701–706, 2023.

[18] Seung Yeong Cho, Gwang Yong Shin, and Do Sik Shim. Effect of laser remelting on the surface characteristics of 316l stainless steel fabricated via directed energy deposition. *Journal of Materials Research and Technology*, 15:5814–5832, 2021.

[19] Francesco Bruzzo, Guendalina Catalano, Ali Gökhan Demir, and Barbara Previtali. Surface finishing by laser re-melting applied to robotized laser metal deposition. *Optics and Lasers in Engineering*, 137:106391, 2021.

[20] Daniyar Syrlybayev, Aidana Seisekulova, Didier Talamona, and Asma Perveen. The post-processing of additive manufactured polymeric and metallic parts. *Journal of Manufacturing and Materials Processing*, 6(5):116, 2022.

[21] ISO. Geometric product specification (gps) — surface texture: Profile - part3: Specification operators. Standard ISO 21920-3:2021, ISO, Geneva, Switzerland, 2021.

[22] Chang Ye, Chaoyi Zhang, Jingyi Zhao, and Yalin Dong. Effects of post-processing on the surface finish, porosity, residual stresses, and fatigue performance of additive manufactured metals: a review. *Journal of Materials Engineering and Performance*, 30:6407–6425, 2021.

[23] Gary S Schajer. *Practical residual stress measurement methods*. John Wiley & Sons, 2013.

[24] MN James, DJ Hughes, Z Chen, H Lombard, DG Hattingh, David Asquith, JR Yates, and PJ Webster. Residual stresses and fatigue performance. *Engineering Failure Analysis*, 14(2):384–395, 2007.

[25] NS Rossini, Michele Dassisti, KY Benyounis, and Abdul-Ghani Olabi. Methods of measuring residual stresses in components. *Materials & Design*, 35:572–588, 2012.

[26] Alberta Aversa, Gabriele Piscopo, Alessandro Salmi, and Mariangela Lombardi. Effect of heat treatments on residual stress and properties of aisi 316l steel processed by directed energy deposition. *Journal of Materials Engineering and Performance*, 29(9):6002–6013, 2020.